https://doi.org/10.5194/egusphere-2023-1234
Preprint. Discussion started: 19 June 2023
© Author(s) 2023. CC BY 4.0 License.

Version of June 7, 2023

Radiative impact of thin cirrus clouds in the lowermost stratosphere and tropopause region

Reinhold Spang[1], Rolf Müller[1], and Alexandru Rap[2]

[1]Forschungszentrum Jülich GmbH, IEK-7, 52425 Jülich, Germany
[2]School of Earth and Environment, University of Leeds, Leeds LS2 9JT, United Kingdom

Correspondence: Reinhold Spang (r.spang@fz-juelich.de)

Abstract. Cirrus clouds play an important role in the radiation budget of the Earth. Despite recent progress in remote sensing observations of cirrus in general, the radiative impact of thin cirrus clouds in the tropopause region and in the lowermost stratosphere remains poorly constrained. This is due to their small vertical extent and optical depth, which make them very difficult to observe for most instruments. In addition, their shortwave (cooling) and longwave (warming) radiative effects (RE) are often in approximate balance, which together with uncertainties regarding the shape and size of cirrus particles, make their overall impact on climate difficult to quantify.

In this study the SOCRATES (Suite Of Community RAdiative Transfer codes based on Edwards and Slingo) radiative transfer model was used to calculate the shortwave and longwave RE for observed thin cirrus during the second space shuttle mission by the CRyogenic Infrared Spectrometers and Telescopes for the Atmosphere (CRISTA-2) instrument. Unusual high cloud top heights with respect to the tropopause and rather high occurrence rates have been retrieved in earlier studies. However, the question remained open if these optically ultra thin cirrus clouds (UTC), so far not considered in global model calculation, are of importance for the Earth's radiation budget.

Using sensitivity simulations with different ice effective particle size and shape, we provide an uncertainty range for the RE of UTCs in the lowermost stratosphere and tropopause region during both summer and winter months. Cloud top height and ice water content are based on CRISTA-2 retrievals, while the cloud vertical thicknesses were assumed to be 0.5 or 2 km. Our results indicate that if the ice crystals of these thin cirrus clouds are assumed to be spherical, then their net RE is generally positive (warming). In contrast, if they are assumed to be aggregates, a less likely habit for this high altitude cirrus type, then their net RE is generally negative (cooling) during summer months and positive (warming) during winter months. The cooling or warming RE is in the order of $\pm$(0.1-0.01) W/m^2 for a realistic global cloud coverage of 10%, similar to the magnitude of the contrail cirrus radiative forcing best estimate of $\sim$0.1 W/m^2. RE is also dependent on the cloud vertical extent and consequently the optically thickness and effective radius (R_{eff}) of the particle size distribution (e.g. R_{eff} increase from 10 to 30 μm results in a factor $\simeq 3$ smaller short and longwave effects). We argue that the radiative impact of UTC clouds in the lowermost stratosphere and tropopause region needs to be better addressed in observations and need to be taken into account in climate simulations.

https://doi.org/10.5194/egusphere-2023-1234
Preprint. Discussion started: 19 June 2023
© Author(s) 2023. CC BY 4.0 License.

1 Introduction

Cirrus clouds are an important contributor to the radiation budget of the Earth (e.g., Liou, 1986; Heymsfield et al., 2017). While there has been recent progress in understanding cloud formation processes, aerosol-cloud interactions, and cirrus cloud radiative effects, cirrus clouds are still one of the major uncertainties in climate model projections (Forster et al., 2021).

The classification of different cirrus cloud classes with respect to optical thickness (τ) has been defined by Sassen and Cho (1992) and is based on lidar observations at visible wavelengths, where an optically thick cloud is defined for $\tau > 3$, opaque cirrostratus for $0.3 < \tau < 3$, transparent or thin cirrus for $0.03 < \tau < 0.3$, and subvisible cirrus (SVC) for $\tau < 0.03$. More recent observations with infra-red limb sounders found even optically thinner cirrus clouds in the range $10^{-6} < \tau < 10^{-2}$ in the tropopause region and partly significantly above the tropopause (Spang et al., 2002, 2008, 2015; Zou et al., 2020; Bartolome Garcia et al., 2021). These observations were obtained by space and airborne limb sounders. These clouds have been also detected by in situ particle measurements (Krämer et al., 2016) but are only observable to a moderate extent by space borne lidars (Davis et al., 2010; Spang et al., 2015). To better discriminate the optically extremely thin clouds from most of the cirrus defined above, these clouds are referred to in the following as ultra thin cirrus (UTC), which is in line with the optical thickness definition ($\tau = 10^{-3}\,\text{to}\,10^{-4}$) of the ultrathin tropical tropopause cirrus (UTTC) (Peter et al., 2003) detected with airborne lidar and in situ particle measurements.

Assuming UTCs at the tropopause to be a common cloud type, the question arises about the radiative effect (RE) of these clouds – cooling or warming. The imprint of UTCs on the radiative net effect of cirrus is not well constrained due to the difficulties to characterise microphysical as well as macrophysical quantities of UTCs. Hong et al. (2016) reported a detailed analysis on RE over a wide range of optical thickness of ice clouds based on space borne Cloud–Aerosol Lidar and Infrared Pathfinder Satellite Observations (CALIPSO) lidar and CloudSAT radar data. They computed the cirrus radiative effect (CRE) for a global multiyear climatology of retrieved ice water content, effective radius, and extinction covering low-level optically thick to high-level thin cirrus clouds. For the 2008 period, they found the warming effect (21.8 W/m^2) induced by ice clouds trapping longwave radiation exceeds their cooling effect (16.7 W/m^2) caused by shortwave reflection, resulting in a net warming effect (5.1 W/m^2) globally on the earth–atmosphere system. But the study does not include the optically thinnest cirrus (UTCs), which are hard to detect and may systematically underestimated in the dataset. Davis et al. (2010) showed the difficulties to observe optically very thin cirrus clouds around the tropopause with the CALIOP lidar in comparison to in situ particle measurements. The analysis suggests that a majority (>50%) of SVCs around the tropopause ($\tau < 0.01$) could be unaccounted for in studies using CALIPSO data. Consequently, Hong et al. (2016) show only data for $\tau > 0.01$.

A more recent analysis of stratospheric ice clouds (SIC) based on the CALIOP cloud product shows rather high occurrence frequencies (2-20%) nearly all over the globe (Zou et al., 2020, 2022), with maxima in the tropics but local maxima at mid latitudes at the storm track regions, with a preference for the tropics but reasonable occurrence frequencies at mid and high latitudes (2-10%). In addition, the CALIOP shows less SICs at mid-latitudes than the Michelson Interferometer for Passive Atmospheric Sounding (MIPAS) on the Envisat satellite (IR-limb sounder) if both data sets are normalized in the tropics (Zou et al., 2020). Cirrus cloud occurrence frequencies retrieved with the CRyogenic Infrared Spectrometers and Telescopes for the

https://doi.org/10.5194/egusphere-2023-1234
Preprint. Discussion started: 19 June 2023
© Author(s) 2023. CC BY 4.0 License.

Atmosphere (CRISTA) instrument showed for the first time on global scales significant numbers of cirrus occurrence at and above the tropopause (Spang et al., 2002, 2015) and present IR limb sounder as one of the most sensitive measurements for the detection of cirrus clouds. Due to its better vertical resolution than MIPAS these data allow a better and more sophisticated quantification of the radiative effect of the proven optically thinnest cirrus clouds. The study is structured in the following way: Section 2 describes the instrument data and corresponding analyses and retrievals for setting up most realistic optically thin cloud profiles in the tropopause region at mid and high latitudes. Section 3 presents radiative transfer calculations with the SOCRATES model and the results in context of the warming and cooling potential of the corresponding macro and micro physical cirrus characteristics, followed by a discussion regarding the overall cloud radiation effect of the specific cirrus types.

2 Data sets and methodology

2.1 CRISTA instrument

The CRISTA instrument was flown twice on space shuttle missions in 1994 and 1997 in a free-flyer configuration (Offermann et al., 1999; Grossmann et al., 2002). During both missions the instrument made around 8 days of nearly global measurements in the mid-IR (5-15 micron), with still today an unprecedented horizontal resolution for a limb sounder. This was possible by the implementation of three telescopes with crossing viewing directions, which results in a rather dense measurement net (Fig. 1) - even in the tropics (not presented). With an along track sampling of 200/400 km and three viewing directions the typical gaps between the orbits in the equator and mid-latitude region are filled with measurements. Additionally, the pointing capability of the satellite allowed CRISTA-2 to extent the latitudinal coverage up to 74°N/S away from the more restricted coverage defined by the orbit inclination of 57° (fixed value for CRISTA-1 coverage). The rather good vertical resolution and sampling of 1.5 km and 2.0 km respectively, helps cirrus clouds to be detected and the exact location with respect to the tropopause to be determined with rather high accuracy (Spang et al., 2002, 2015).

The typical horizontal averaging along the line of sight of a limb sounder is in the order of 200-300 km, where the narrow field of view helps to keep this uncertainty in an adequate range but this limits the accuracy of the retrieved limb ice water path (IWP) (see also Sec 2.3 for details) from CRISTA. Where along the line of sight the cloud is located, and more important, how long the path length through the cloud is, can not be retrieved because of the CRISTA limb geometry. Although, these are typical caveats for cloud and trace gas retrievals of limb sounders, modified instruments like limb imager allow substantial improvements of macroscopic cloud parameter with refined observation and retrieval techniques (e.g. 2D/3D and tomographic retrieval techniques, Ungermann et al., 2020). However, the CRISTA measurement capabilities are still unique for the limb IR technique. Extremely low cloud optical thicknesses are detectable which results in a very high detection sensitivity for IWC ($> 5 \cdot 10^{-6} g/m^3$), vertical IWP ($2 \cdot 10^{-4}$ g/m^2), and extinction ($8 \cdot 10^{-4} - 10^{-2}$ km^{-1}) (Spang et al., 2012, 2015). The latter extinction values constitute the upper limit of the measurement range of IR limb sounders. For extinctions $> 10^{-2}$ km^{-1} the IR spectrum saturates and becomes optically thick in the limb and the instrument loses sensitivity for optically thicker clouds.

https://doi.org/10.5194/egusphere-2023-1234
Preprint. Discussion started: 19 June 2023
© Author(s) 2023. CC BY 4.0 License.

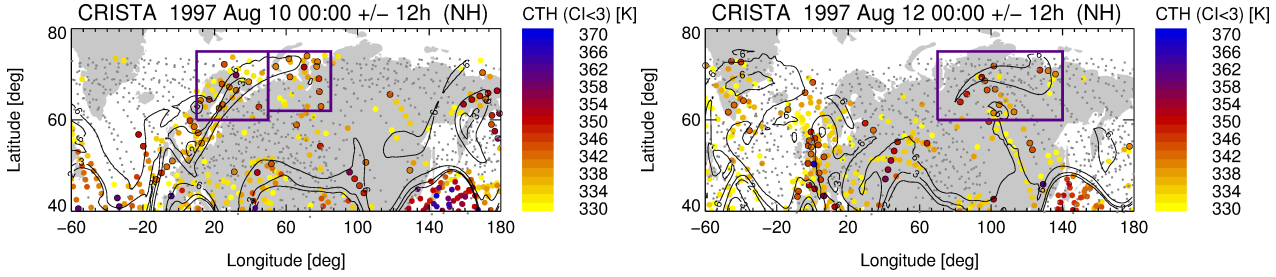

Figure 1. Regions of interest with high altitude cirrus clouds coverage for August 10 and August 12 1997 with high altitude cirrus clouds. The maps are adapted from Spang et al. (2015). Cloud top heights(CTH) are given in potential temperature coordinates. Colored symbols with a black circle are highlighting CTHs above the lapse rate tropopause based on ERA5 reanalysis data and CRISTA-2 cloud observations.

2.2 SOCRATES radiation model

Radiative flux calculations have been performed using the offline version of the SOCRATES (Suite Of Community RAdiative Transfer codes based on Edwards and Slingo) radiative transfer model (Edwards and Slingo, 1996) with six bands in the shortwave (SW), nine bands in the longwave (LW) and a delta-Eddington two-stream scattering solver at all wavelengths. This version has been used extensively in previous studies for calculating radiative effects from several atmospheric agents, including contrails (e.g. Myhre et al., 2009a; Rap et al., 2010), water vapour (e.g. Myhre et al., 2009b; Riese et al., 2012; Kunz et al., 2013), ozone (e.g. Rap et al., 2015a; Riese et al., 2012), or aerosols (Rap et al., 2013, 2015b, 2018).

The model simulates ice clouds radiative effects using the Baran et al. (2014) parameterisation for ice clouds bulk optical properties. Radiative flux calculations are performed for specified ice cloud fraction, ice crystal effective radius and mass mixing ratio. Spherical or aggregate ice crystal shapes can be simulated based on the Baran (2003) database of aggregates, using 83 representative size distributions measured during the CEPEX campaign. The diurnal variations in the SW are simulated by calculating the daily average SW radiative effects based on 24 instantaneous values (i.e. model runs with a 1-hour time resolution) using pre-calculated solar zenith angles (SZAs) at profile location.

2.3 Data preparation and model setup

In order to guide the model in a realistic clouds parameter space, the simulations were set up based on the CRISTA-2 measurements. IWC and extinction estimates, as well as accurate cloud top heights with respect to the tropopause height, are retrieved from the satellite and meteorological reanalysis datasets. ECMWF's fifth-generation reanalysis, ERA5 (Hersbach et al., 2020), is used for temperature, ozone and specific humidity information at the profile location of CRISTA-2. Additionally, ERA5 pressure and geopotential height are applied to transform between the vertical coordinate altitude for the satellite and pressure levels for the model. The derivation of lapse rate tropopause height and pressure from ERA5 is following the method of Hoffmann and Spang (2022).

https://doi.org/10.5194/egusphere-2023-1234
Preprint. Discussion started: 19 June 2023
© Author(s) 2023. CC BY 4.0 License.

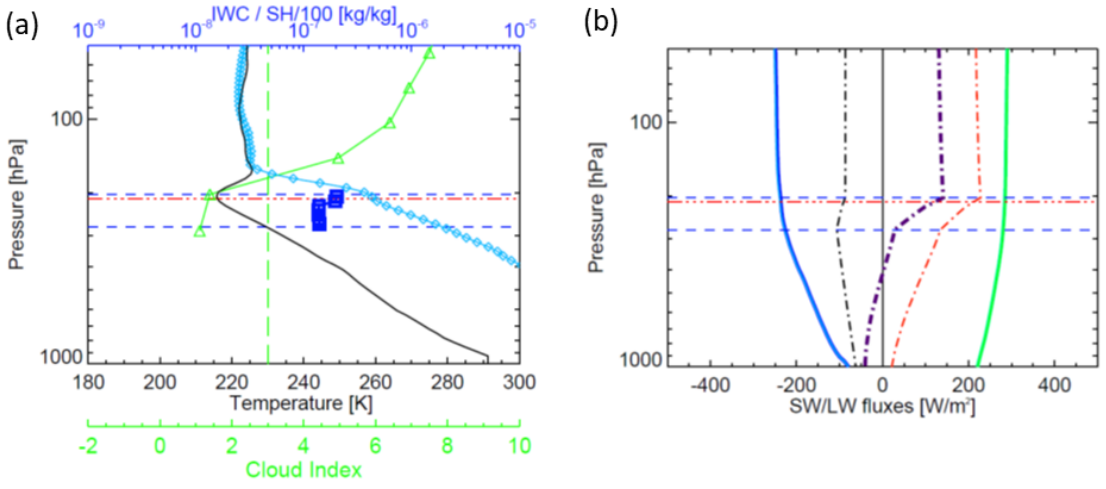

Figure 2. (a): Input profiles for the SOCRATES model runs for the 9th August 1997 13:47:13, 23.2°E and 68.6°N, with temperature (black) and SH (light blue) from ERA5, IWC (blue) retrieved for CRISTA-2 and additional information like the cloud index profile for cloud detection (CI, in green and threshold value CI=3 dashed green line) as well as cloud top and base height (blue dashed) and ERA5 based lapse rate tropopause (red dash-dotted) (following Hoffmann and Spang, 2022). All information are interpolated on the SOCRATES pressure grid. **(b):** Output profiles on SW (blue) and LW (green) all-sky and clear-sky fluxes by the model. The difference of all-sky and clear-sky (SW-black and LW-red) and the sum of SW and LW (purple) are shown by dash-dotted lines and are scaled by a factor of 100. Top of atmosphere total radiative effect result to RE_{SW}+RE_{LW} = -0.86 + 2.14 = 1.28 W/m^2.

The cloud detection capabilities and the high detection sensitivity for cirrus clouds by IR limb sounders, have been demonstrated in various studies (Spang et al., 2002; Massie et al., 2010; Spang et al., 2015; Zou et al., 2020) and for various instruments. The detection method is based on a color ratio of the emissions in a CO_2 and minor ozone band at a wavenumber region around 792 cm^{-1} and an atmospheric window region at 830 cm^{-1}. The so-called cloud index (Spang et al., 2004) is high (CI>4) for optically thin and cloud free conditions and is shrinking to values close to one when getting optically thick in the limb direction. We applied a cloud index threshold of 3 for cloud top height detection, a robust threshold, applied and evaluated in various studies (e.g. Spang et al., 2004, 2012). The method was developed originally for the CRISTA satellite instrument but has been successfully adopted due to its high efficiency to other IR limb sounder, like the Michelson Interferometer for Passive Atmospheric Sounding (MIPAS) instrument (Fischer et al., 2008) on the Envisat satellite (Spang et al., 2004, 2012; Zou et al., 2020) or more recently on airborne instruments (Spang et al., 2008; Bartolome Garcia et al., 2021).

The CRISTA observations are used to define the macro and microphysical cloud parameter required for the SOCRATES run. In total 161 profiles with cirrus clouds around the tropopause have been selected form the CRISTA-2 dataset in the regions highlighted in Fig. 1. Spang et al. (2012) showed, that the cloud index value in the optical thin part of cloud measurement correlates well with the limb integrated surface area density along the limb path (ADP) (equivalent to a limb IWP) and generated look-up tables for various altitudes and latitudes. In addition, taken the effective radius of the particles into account (predefined

https://doi.org/10.5194/egusphere-2023-1234
Preprint. Discussion started: 19 June 2023
© Author(s) 2023. CC BY 4.0 License.

for the model runs with 10 and 30 μm) it is possible to estimate the mean IWC along the line of sight under the assumption of a tangent height layer homogeneously covered by the cirrus cloud. A constant path length through the cloud of 200 km has been applied. Usually, the path length depends on the tangent point altitude with respect to the real cloud top (not the detected instrument based cloud top height, because of the limited vertical resolution and sampling of the instrument the real CTH can be lower or higher than the detected CTH). In addition, the cloud path length depends on the size of the field of view. Consequently, for a horizontally and/or vertically large cloud extent the limb cloud path can become extremely long (150 to 400 km for 1 to 3 km respectively vertical resolution). In the current analysis, we are mainly interested in the cloud top region, up to 1-2 km below the cloud top, where the cloud is usually still optically thin and an effective cloud path of $\simeq$200 km is a reasonable assumption for the rather small field of view of 1.5 km of CRISTA (Spang et al., 2012, 2015). In summary, IWC is estimated from the retrieved CTH and ADP or the ADP-equivalent limb IWP, where the effective radius and cloud thickness (Δz) are predefined (0.5 and 2 km). The CRISTA measurements were taken in August 1997, which means under rather high solar zenith angle conditions with many hours of sunlight. For contrast we mirrored the CRISTA observation to February conditions to simulate contrapuntal winter-like events with respect to meteorological (ERA5) and solar conditions.

Particle shape and roughness are very important parameters for correctly modelling the radiative effect of cirrus clouds (Yi et al. (2013), and references therein). Cirrus particles can have very complex particles shapes (for a review see Lawson et al., 2019). Various studies show less complexity for the cold cloud top regions, especially in the tropical tropopause region where quasi spherical particles with radii smaller than 50 μm seems to dominate the particle size distribution and complex ice aggregates are less frequently observed (Woods et al., 2018). It is reasonable that cirrus at the tropopause and lower stratosphere (cloud top) at mid and high latitude have also less complex shapes than optically thick ice clouds in the free troposphere. In this study we decided to use the scattering properties of two extreme particle shapes: (a) aggregates, a specific composition of ice crystal habits (Baran, 2003; Baran et al., 2014, 2016; Yang et al., 2005), and in contrast (b) spherical ice particles as a simplification for the in situ measurements observed quasi-spherical particles in the cloud top region, which are typically best described by droxtals (Yang et al., 2003; Zhang et al., 2004) or Chebyshev particles (Rother et al., 2006; McFarquhar et al., 2002).

Cloud optical depth (τ) is an important parameter when investigating the cooling or warming potential of cirrus clouds (e.g. Hong et al., 2016). We computed τ from the CRISTA cirrus cloud detections by the CI-IWC relation prepared in look up tables of ADP or limb IWP versus CI with respect to cloud altitude and a further correlation between extinction k_e and IWC/R_{eff} with $k_e = const \cdot \text{IWC}/R_{\text{eff}}$, with $const = 1.4 \cdot 10^3$, IWC in g/m^3, R_{eff} in μm, and k_e in km^{-1} (Spang et al., 2012). Finally, a simple integration of k_e over the cloud layer thickness (Δz) results in the vertical optical depth $\tau = \int k_e dz$ which is used for the SOCRATES input (Figure 3). The CRISTA based optical depth (Figure 3b) covers the full range of UTCs from extremely low $\tau < 0.001$ up to a maximum of $\tau \simeq 0.05$, which is still in the range of SVCs.

For comparison an estimate of the optical depth $\tau = 1.5 \cdot \text{IWP}/(\rho_{\text{ICE}} \cdot R_{\text{eff}})$ (e.g. Baran and Francis, 2004) with R_{eff} in μm and ρ_{ICE} the mass density of ice in g/cm^3 was also applied to the data. Although, the formula is only strictly correct for ultra violet and visible wave lengths, Baran and Francis (2004) argued that the formula is a reasonable approximation in the infrared region as well, if the ice crystals are sufficiently large and the absorption is strong (e.g. around 11 μm). PDFs of retrieved

https://doi.org/10.5194/egusphere-2023-1234
Preprint. Discussion started: 19 June 2023
© Author(s) 2023. CC BY 4.0 License.

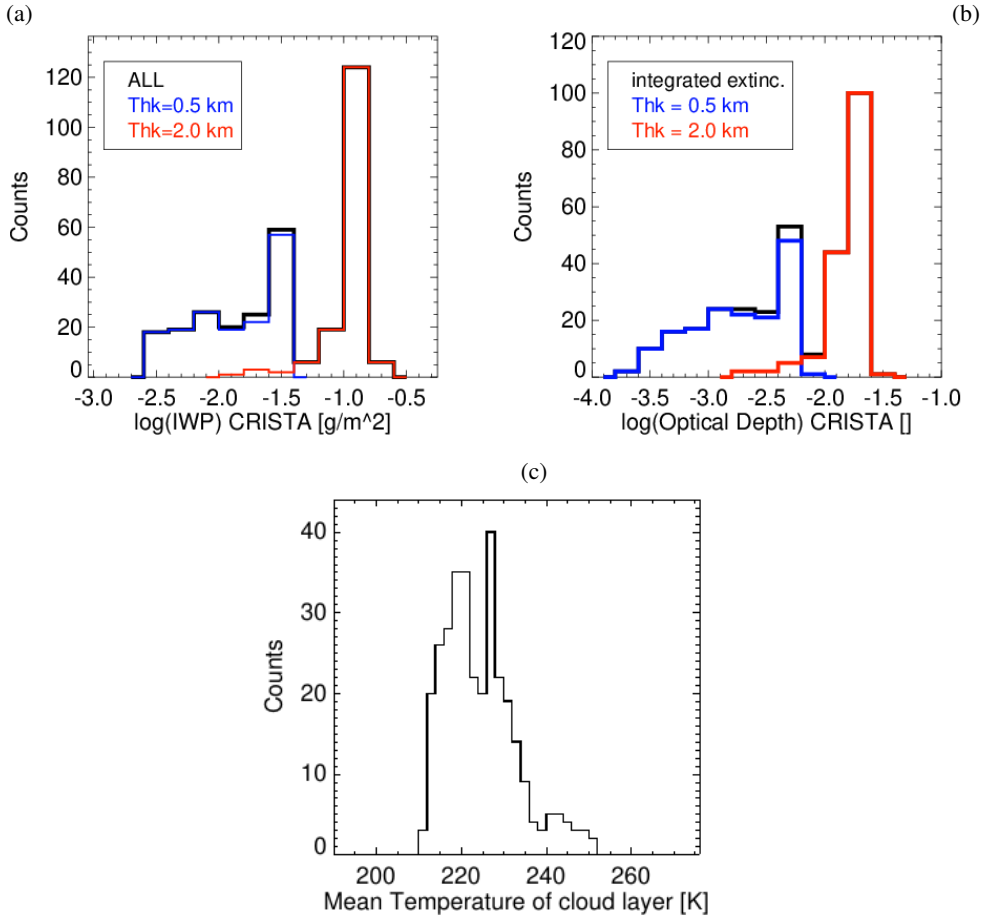

Figure 3. CRISTA based ice water path (a) and optical depth (b) distribution applied to the SOCRATES runs for Δz=0.5 km (blue) and Δz=2.0 km (red) and all together in black). (c) PDF of the mean cloud temperature used in the study for August conditions (ERA5 1997 data).

(Fig. 3a) and estimated (not shown) τ are looking very similar, which gives us confidence that the retrieved IWC, IWP and extinctions are in a reasonable range. Figure 3a and b show the distribution of IWP and optical thickness retrieved from the CRISTA data. The similarities in the PDFs highlight the close link between both parameters.

A summary of all different model scenarios for SOCRATES is presented in Tab. 1 together with the mean model results of the cloud radiative effect (CRE) of all CRISTA profiles accounted for in the simulations. An example of the model input profiles (cloud index, temperature, specific humidity, and IWC) and the output profiles of SW and LW flux profiles for all-sky (as) cloudy and clear-sky (cs) none-cloudy conditions are presented in Fig. 2. CRE is defined as the sum of SW and LW effect of the all-sky minus clear-sky fluxes (F) at the top of atmosphere in W/m^2:

$$\mathrm{CRE} = (F_{\mathrm{SW_{as}}} - F_{\mathrm{SW_{cs}}}) + (F_{\mathrm{LW_{as}}} - F_{\mathrm{LW_{cs}}})$$

https://doi.org/10.5194/egusphere-2023-1234
Preprint. Discussion started: 19 June 2023
© Author(s) 2023. CC BY 4.0 License.

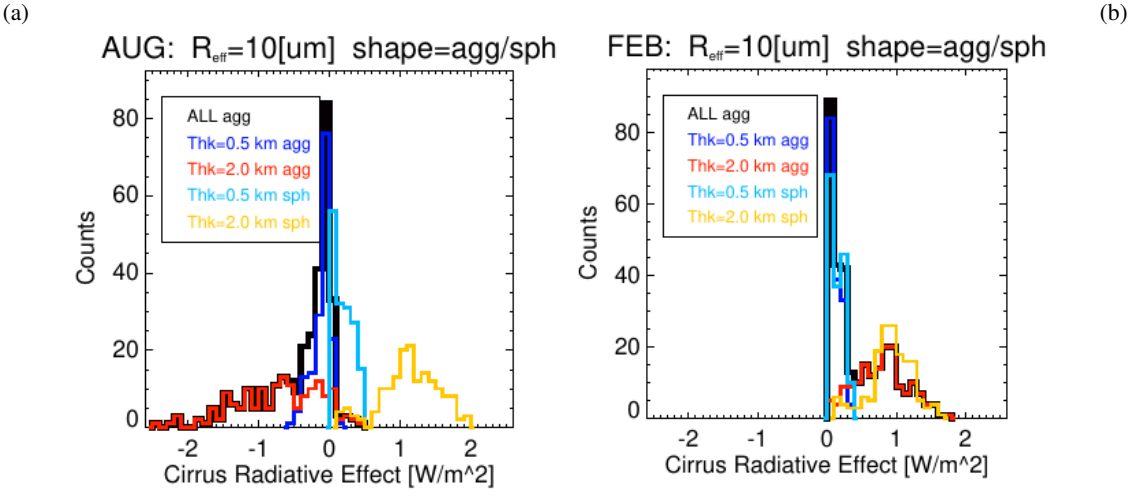

Figure 4. PDFs of CRE for various setups of the SOCRATES runs for 10 μm effective radius of the particles, August (a) and February (b) background atmosphere, for aggregates (black, separated in cloud thickness Δz =0.5 km and Δz =2 km in blue and red) in comparison to spherical particles (0.5/2km in light blue/orange).

LW, SW and total flux (CRE) are saturating above the cloud top (<100 hPa) with virtually constant values (Fig. 2b), and a simple definition of the top of atmosphere (ToA) radiative effect is applicable by means of the pressure levels 20 to 0.6 hPa. The latter pressure value is the minimum pressure level in the model run.

Figure 3a gives an overview of the range and occurrence in the vertical IWP from the CRISTA estimates. The obviously very different vertical cloud thicknesses of 0.5 and 2.0 km result in a separation in the PDF of IWP with very small IWPs between $3 \cdot 10^{-3}$ and $5 \cdot 10^{-2}$ g/m^2 for the 0.5 km cloud layers and an IWP $\simeq 10^{-1}$ g/m^2 for the 2 km extended cirrus. All modelled respectively observed cirrus clouds are optically thin in the limb and nadir direction and will be invisible for most passive nadir instruments. The lowest IWP values are equivalent to an IWC of 10^{-5} g/m^3 which is one order of magnitude larger than the detection sensitivity of IR limb sounders (Spang et al., 2015) and close to the so far lowest IWC values observed in situ measurements (10^{-6} g/m^3, Krämer et al., 2020).

The mean temperature of the modelled cloud layers are for August in the range of 210 to 250 K (Fig. 3c) peaking around 220 K, which is a typical tropopause temperature at this time of season (s. Fig. 2, Hoffmann and Spang (2022)). February temperature profiles have been selected from ERA5 and are not observational based (longitude and latitude of the August cloud observations). The corresponding estimated cloud temperatures are lower than in August (the maximum of the probability distribution peaks at 210 K, not shown). Although the selected temperature profiles for February may not be realistic for the microphysical formation of a cirrus (e.g. frequent CTHs are modelled in February significantly above the tropopause) it seams reasonable to use the profiles for T, SH, and O_3 to define the background atmosphere conditions for February scenarios in SOCRATES.

https://doi.org/10.5194/egusphere-2023-1234
Preprint. Discussion started: 19 June 2023
© Author(s) 2023. CC BY 4.0 License.

Table 1. Median cirrus radiative effect of 161 profiles, as well as separated LW and SW effect in W/m^2 for various scenarios of the SOCRATES runs

Scenario:	AUG	AUG	FEB	FEB	month
shape / R_{eff}	0.5 km	2.0 km	0.5 km	2.0 km	cloud depth
agg / 10 μm	*1*	*2*	*3*	*4*	*Scene ID*
	0.40	2.72	0.19	1.46	LW
	−0.44	−3.44	−0.09	−0.63	SW
	−0.06	**−0.64**	**0.09**	**0.81**	**CRE**
agg / 30 μm	*5*	*6*	*7*	*8*	*Scene ID*
	0.14	1.01	0.07	0.54	LW
	−0.14	−1.17	−0.03	−0.20	SW
	-0.01	**-0.10**	**0.04**	**0.33**	**CRE**
sph / 10 μm	*9*	*10*	*11*	*12*	*Scene ID*
	0.28	1.99	0.14	1.09	LW
	−0.10	−.85	−0.02	−0.15	SW
	0.17	**1.15**	**0.13**	**0.93**	**CRE**
sph / 30 μm	*13*	*14*	*15*	*16*	*Scene ID*
	0.09	0.65	0.05	0.35	LW
	−0.03	−0.27	−0.01	−0.04	SW
	0.06	**0.37**	**0.04**	**0.31**	**CRE**

3 Cloud radiative effect of optically thin cirrus

An overview of CRE of the individual profiles is presented Figure 4 by probability density functions (PDF) for various Δz and particle shapes (color-coded) as well as for August and February background conditions. Obviously, February and August show a contrasting behaviour, with relatively broad distributions of negative CRE for aggregates from -2.5 to 0 W/m^2 changing to positive CRE for spherical particles (+0.5 to 2 W/m^2). For winter conditions all profiles show a positive CRE, not a single event is reaching negative CRE. For $R_{\text{eff}} = 30\,\mu$m the distributions are looking very similar, only the distribution width is roughly half of the smaller particle mode (not shown). The striking change in CRE between winter and summer conditions is now investigated in more detail.

Figure 5 gives a better representation of the SW, LW and net effect with respect to the optical depth (Sec. 2.3) of the modelled clouds. The left column shows CRE versus optical depth for five respectively 10 model scenes, always for Δz = 0.5 and 2 km, August, $R_{\text{eff}} = 10\,\mu$m and $30\,\mu$m, with shape aggregate; August, $R_{\text{eff}} = 10\,\mu$m and $30\,\mu$m with shape spherical; and February, $R_{\text{eff}} = 10\,\mu$m with shape aggregate. The exponential growth of SW and LW effects with increasing $\log(\tau)$ is obvious for all setups, especially well pronounced for the combination of August and aggregates. SW and LW effect are nearly in balance

https://doi.org/10.5194/egusphere-2023-1234
Preprint. Discussion started: 19 June 2023
© Author(s) 2023. CC BY 4.0 License.

and changes in shape or radius can significantly change the net effect (black symbols in Fig. 5 (a, c, e, g, i)) from cooling to warming and vice versa. The interplay of SW and LW effect is visualized in more detail in the right column of Figure 5 (b, d, f, h, and j). Deviations from the one-to-one line are highlighting the warming (above) and cooling (below) of the net (cirrus) radiative effect for each single cloud event modelled with SOCRATES. Smaller Δz induces a very similar ratio between LW and SW effect, illustrated by rather similar gradients and only smaller amplitudes in the LW-SW correlation. For summer conditions and particle shapes of aggregates the short wave scattering effect can reach a very large cooling (extended day length), especially for larger optical depth values ($\tau > 0.01$). This results in the only 4 scenarios (Scene 01, 02, 05 and 06) with an overall cooling potential (AUG, aggregates, R_{eff}= 30 and 10 μm) presented in Figure 5(a-d). However, even smaller effective radii ($< 10\,\mu m$) will result in even larger cooling effects for aggregates or similar complex particle shapes. In situ measurements show for optically thin cirrus clouds (SVC and/or UTC) typically $R_{\text{eff}} <\simeq 100\,\mu$m and quasi-spherical with some plates and rare triagonal shapes (Lawson et al., 2019). Thus, aggregates are not a very plausible particle shape for the optically thinnest cirrus clouds observed by CRISTA.

For spheres instead of aggregates the SW scattering efficiency is less pronounced and cooling effects are generally smaller in amplitude and usually smaller than the LW warming for spheres (Figure 5(e-h)). For winter (FEB) conditions the short wave cooling becomes smaller due to reduced daylight hours (taking also into account the rather high geographical latitudes) which results in a general warming for all winter scenarios and the change from cooling to warming for aggregates with R_{eff}=10μm (Fig. 5 e, f). Enlarged R_{eff} from 10 to 30 μm results in a general reduction of SW and LW effect, but a significantly larger decrease in the SW than the LW (Fig. 5 (g,h)). This gives an overall net cooling of for August profiles of aggregates but with a significant number of warming events compared to the 10 μm scenario (Fig. 5 (c,d)).

There is a strong R_{eff} dependency on the SW, where larger particles correspond to smaller surface area densities for constant IWC and consequently smaller SW scattering. Generally, 0.5 and 2 km cloud layers behave very similar to changes in the parameter settings (LW: orange and red, SW: lilac and blue in Fig. 5). Whereby, τ is a significant factor of 4 smaller for Δz =0.5 than for the Δz =2 km cloud layers.

In addition, we tried to find a relation between CRE and the distance to the tropopause as well the mean cloud top temperature. Figure 6 presents only results for R_{eff} =10 μm (30 μm differs only by a reduction in magnitude and no change in sign) for spherical particles and aggregates. Corresponding CRE versus optical depth like in Figure 5 is presented as well in Figure 6 (e) and (f). By an additional binning along the corresponding y-axis and the computation of median and percentiles per bin, the interquartile range (percentile p75 - p25) is presented as an error bar to better visualize the variability for constant optical depth. Median and interquartile range are better suited than mean and standard deviation to characterize data with high internal variability, extreme outliers, or skewed distributions.

https://doi.org/10.5194/egusphere-2023-1234
Preprint. Discussion started: 19 June 2023
© Author(s) 2023. CC BY 4.0 License.

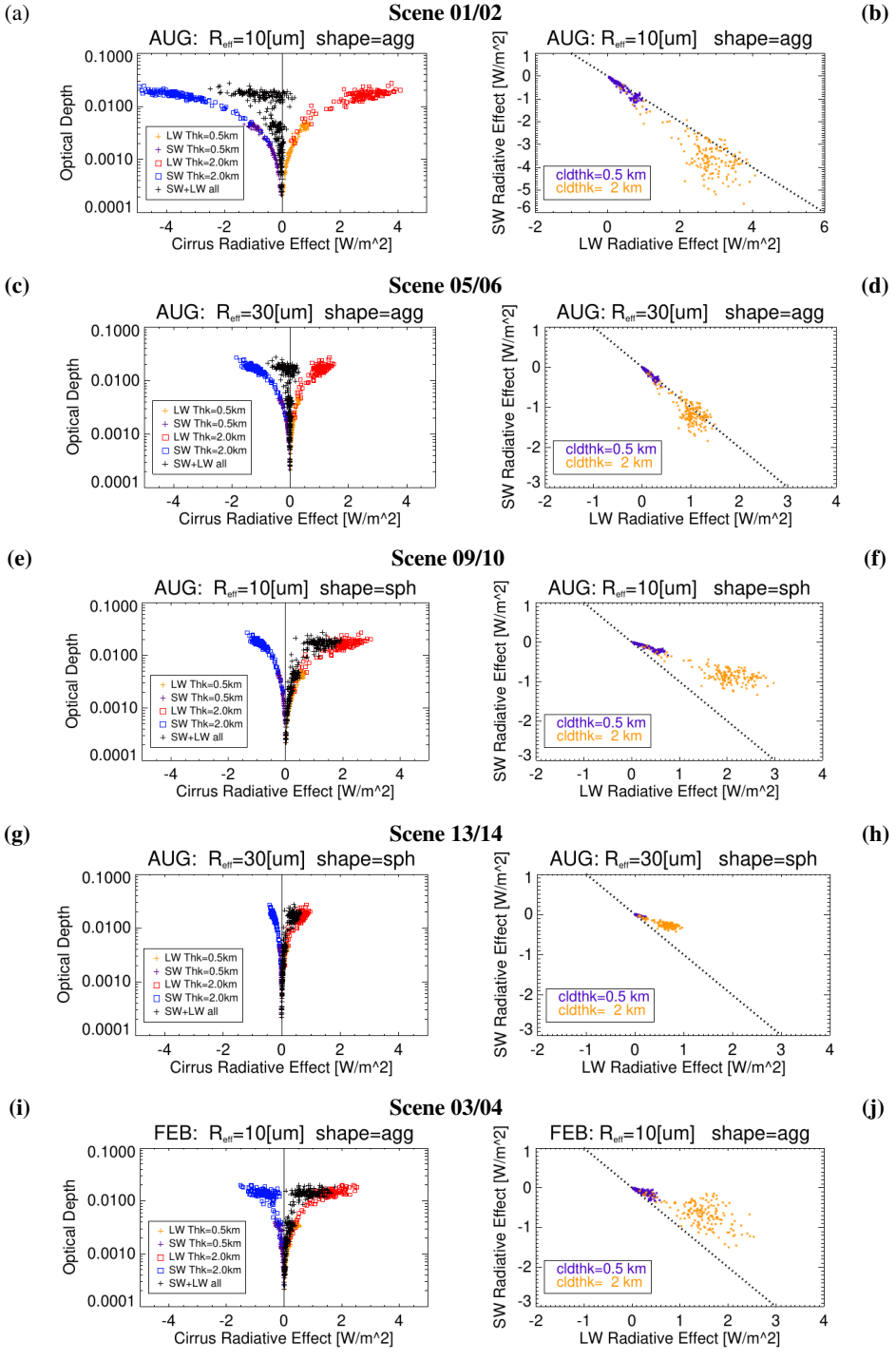

Figure 5. Cirrus radiative effect (colour coded LW, SW and total in blue/purple, red/orange ($\Delta z = 2/0.5$ km) and black) with respect to optical depth (left) and LW versus SW radiative effect (right column) with aggregates in August with $R_{\text{eff}} = 10\,\mu$m (a, b) and $30\,\mu$m (c, d), with spherical particles for August for $R_{\text{eff}} = 10\mu$m (e, f) and $30\,\mu$m, and (g, h), as well as aggregates for February conditions and $R_{\text{eff}} = 10\mu$m (i, j).

https://doi.org/10.5194/egusphere-2023-1234
Preprint. Discussion started: 19 June 2023
© Author(s) 2023. CC BY 4.0 License.

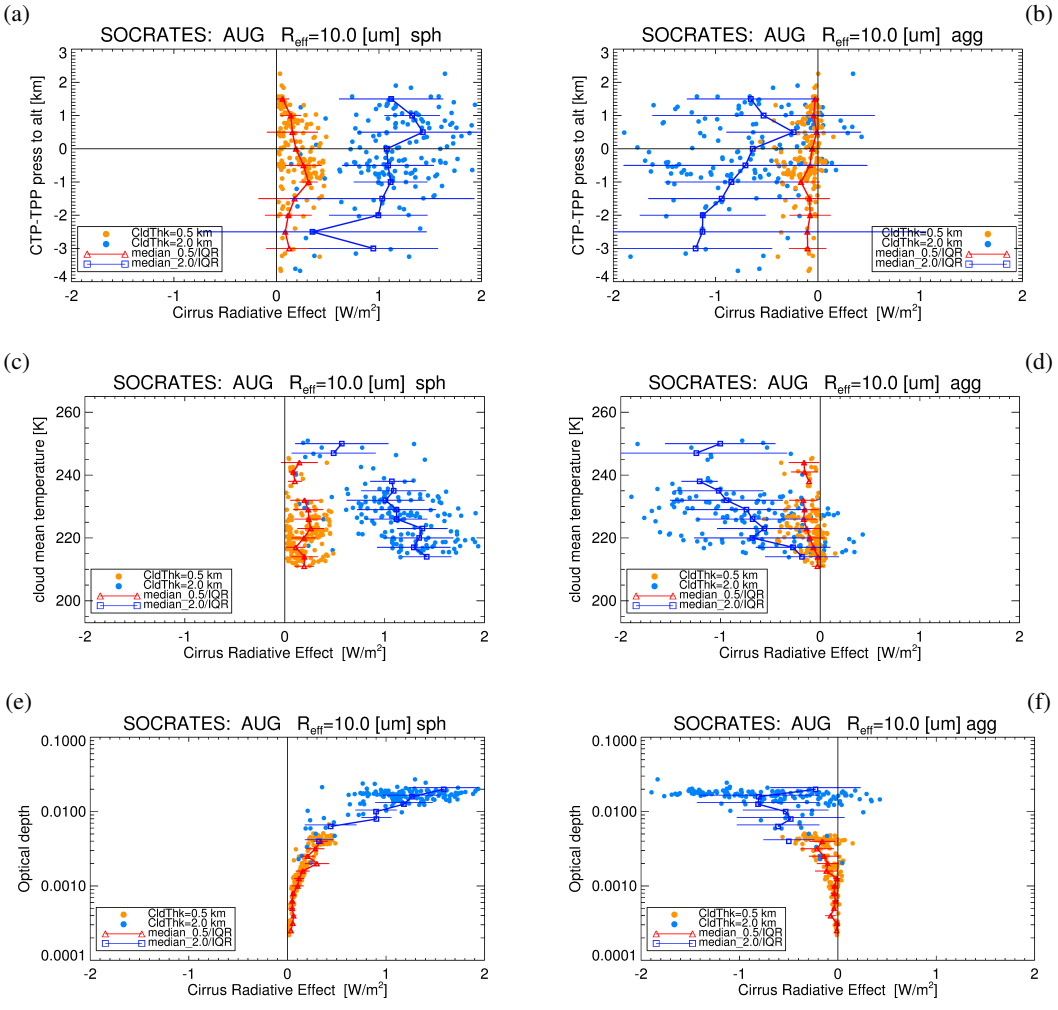

Figure 6. Cirrus radiative effect with respect to the distance to the tropopause (a, b), cloud mean temperature (c, d) and the optical depth (e, f) for August, $R_{\text{eff}} = 10\,\mu$m spherical and aggregate particle shape in the left and right column. The error bars represent the interquartile range.

CRE versus the distance to the tropopause in log-pressure coordinates shows no obvious correlation or trend. The interquartile range is rather large and the distance to the TP seams not to correlate strongly with CRE. However, the median indicates a weak cooling in CRE with larger distances above the tropopause. This is more strongly pronounced for aggregates than for spheres, and only significant for 2 km cloud thickness. Δz =0.5 km events show smaller tendencies, in the range of -1 km to 3 km with respect to the tropopause the gradient looks for aggregates even opposite to spheres. So far there is no explanation found for this behaviour. Below the tropopause ($\simeq -1.5$ km) the gradient is negative for most of the scenarios.

Mean cloud temperature should have an imprint on CRE, because the emitted radiation of the cloud is directly related to the temperature. One of the major radiation effects by high cold clouds is a warming potential due to the emission at

https://doi.org/10.5194/egusphere-2023-1234
Preprint. Discussion started: 19 June 2023
© Author(s) 2023. CC BY 4.0 License.

lower temperatures around the tropopause (Heymsfield et al., 2017). Although, in Figure 6c and d, the scatter is still large, the Δz =2 km clouds nicely show a larger mean LW warming with colder cloud temperatures, which results in the observed negative gradient for CRE. The Δz =0.5 km clouds give some indications for a similar pattern with significantly smaller amplitudes, but only aggregates show a mean negative gradient. Again, the sign of CRE for the different setups is not changing over the analysed altitude range.

Finally, CRE versus optical depth is presented similar to Figure 5 but now including the binning for τ with interquartile range and median. The median follows for spherical particles the exponential increase in CRE from the 0.5 and very low τ over the 2 km scenarios to $\tau \simeq 0.02$ and CRE up to 2 W/m^2, whereby the aggregates show the nearly opposite behaviour in CRE, with smaller amplitude and larger scatter (interquartile range error bars).

3.1 Statistics of modelled cloud radiative effect

Table 1 summarises all SOCRATES setups and mean results on LW, SW and net radiative effect. The median values of the selected areas (Sec. 2.3) give distinctive tendencies of the overall cloud warming or cooling effect for the UTCs. In total 161 cloud profiles have been selected from the CRISTA-2 data and represent variable conditions where optical thin cirrus clouds were formed at and above the tropopause north of 60°N. Using more realistic cloud occurrence frequencies would allow a more realistic assessment of the CRE of the UTCs.

The LW effect of scattering and trapping the IR radiation back into the direction of the ground is dominating the SW cooling effect for most of the model scenes. For spherical particle shapes all scenarios, Winter and Summer, result in a net warming effect in the range of 0.17 to 1.15 W/m^2 (AUG) and 0.13 to 0.93 W/m^2 (FEB) for R_{eff}=10 μm. These are generally larger values than the mean effects for aggregates, especially for Summer conditions.

The LW warming is even more effective for larger particles where the resulting smaller surface area densities reduce the SW cooling. However, the SW cooling is also more effective for larger particles. Tab. 1 shows this fact for all simulations of spherical particle and 10 and 30 μm effective radius with ~3 times higher SW and LW effect for the 10 μm effective radius.

The shortwave scattering effect depends strongly on the solar zenith angle and the duration of sunlit hours. For winter conditions the mean SW effect cannot compensate the LW effect for aggregates and spheres, whereby for summer conditions the aggregates can change the sign for CRE from warming to cooling. SW is enlarged from -0.63 to -3.44 W/m^2 and results in a mean CRE of +0.81 (FEB) to -0.64 W/m^2 (AUG). This change of sign – from warming to cooling – does not appear for spherical particles. In contrast to aggregates the CRE stays positive from Winter to Summer and shows even slightly enhanced CRE (e.g. 0.93 to 1.15 W/m^2 for 10 μm and Δz =2 km). The SW effect of spherical particles is by far smaller than the one for aggregates.

4 Discussion

Various settings of UTC clouds have been modelled with SOCRATES for a first quantification of cloud radiative effect of UTCs at mid and high latitudes. The original CRISTA-2 data have already been analysed regarding the cloud occurrence with

https://doi.org/10.5194/egusphere-2023-1234
Preprint. Discussion started: 19 June 2023
© Author(s) 2023. CC BY 4.0 License.

respect to the tropopause by Spang et al. (2015). However, the CRE was not analysed for these unexpected observations of UTCs well above the tropopause and with unprecedented high occurrence rates at high northern latitudes. A comprehensive study was missing where the cooling or warming potential of these clouds is investigated.

For larger effective radii as well for vertical thinner cloud layers (0.5 km) we observe smaller cooling and warming effects in the mean SOCRATES results (Tab.: 1 and Sec. 3.1). The determination of Δz would be an important parameter for a better future quantification of the CRE of UTCs. So far, there is no validated statistical information of the cloud thickness of UTCs available. Although the CALIOP data may miss a rather large part of the optically thinnest UTCs (Davis et al., 2010), the dataset is still the best set available for such an analysis. Zou et al. (2020, 2021, 2022) have analysed cloud occurrence of stratospheric ice clouds (SICs) based on CALIOP data products. The Zou et al. studies have not focused on the vertical extent of these clouds. Zou et al. (2020) showed for mid latitudes that the IR limb measurements by MIPAS give higher occurrence rates on SICs than CALIOP, if both cloud occurrence frequencies are normalised in the tropics. This supports the notion that IR limb sounder are under specific conditions more sensitive in the detection of cirrus cloud than recent lidar in space instruments. This circumstance was already discussed in earlier studies (Spang et al., 2012, 2015; Bartolome Garcia et al., 2021).

The best information on the Δz of UTCs retrieved from IR limb measurements is the more recent analysis of Bartolome Garcia et al. (2021) with data from the GLORIA (Gimballed Limb Observer for Radiance Imaging of the Atmosphere) instrument (Riese et al., 2014) during the airborne campaign WISE (Wave-driven ISentropic Exchange) in the North Atlantic in September/October 2017. Due to the excellent vertical resolution and fine sampling using a 2D infrared imaging detector, the data achieve a vertical sampling and resolution of 140 m. For the first time cloud bottom information was retrieved from extinction profiles.

The analysis shows that in the region investigated by WISE there is a maximum likelihood in cloud extent Δz of 500-625 m with likelihoods for $\Delta z > 1.5$ km of less than 25% of the peak likelihood and in total only 10% of all measured cloud events (Bartolome Garcia et al., 2021, Figure 8a). Note that for a typical Δz of 0.5 to 1 km a lower CRE is calculated than for $\Delta z = 2$ km (Figure 5). Generally, optical depth is a good estimator for the strength of the CRE even at very low optical depth, but the cloud vertical extent is obviously a critical parameter for τ and CRE and there seams a functional relation between CRE, Δz, and τ, respectively (Figure 5).

Cloud top heights with respect to the tropopause show a week correlation with CRE in the SOCARTES results especially below the tropopause with a decrease in mean CRE with warmer cloud temperatures (Figure 6c, d). The variability in the net effect is very large (profile to profile variability), which makes a it difficult to draw a final conclusion on a mean effect with cloud top position with respect to the tropopause, but we found indications for an enhanced warming effect for optically thicker events at higher altitudes with respect to the tropopause .

The CRE is not only affected by τ but the atmospheric background conditions (temperature profile, CTH location, surface albedo, microphysical quantities) can result in conditions, where even similar background conditions and constant τ result in very different CRE. This makes the prediction of a net cooling or warming difficult. Even LW and SW effect turn out to be very different depending on the optical depth (Figure 5). Global measurements with a sophisticated occurrence frequency statistic,

https://doi.org/10.5194/egusphere-2023-1234
Preprint. Discussion started: 19 June 2023
© Author(s) 2023. CC BY 4.0 License.

where the cloud detection is weighted with the covered area the by clouds, are necessary. The subsequent radiation model runs would then allow the overall CRE of UTCs in the tropopause region to be better quantified.

Hong et al. (2016) followed a very similar procedure with the combined CALIPSO/CloudSAT ice cloud data products (DARDAR: Delanoë and Hogan (2008) and 2C-ICE: Deng et al. (2010)). These data may not include the correct amount of UTCs due to a lack of detection sensitivity (see Sec. 1) and will consequently underestimate to some extent the total cloud coverage/occurrence of cirrus clouds. The Hong et al. results are presented for ice cloud optical depths $\tau > 10^{-2}$, a value where the limb measurements are starting to saturate. The Hong et al. analysis lacks the optically thinnest range of $\tau = 10^{-4} - 10^{-2}$ where IR limb sounders are most sensitive. A combination of IR limb and space lidar measurements would be an excellent combination to cover the full range of optical depth of cirrus clouds ($\tau = 10^{-4}$ to > 20) for a comprehensive view on the cirrus radiative effect. Hong et al. (2016) argue that subvisual cirrus ($\tau < 0.03$) display only weak SW and LW radiative effects because of their infrequent occurrence (global mean<5%, Hong and Liu, 2015) and this results in a global mean value of CRE = 0.05 W/m^2 (Hong et al., 2016, Table 4). However, as already argued above, the applied cloud dataset misses a significant number of UTCs and the overall radiative effect for SVCs and UTCs is underestimated. Our study shows that these additional UTC radiative effect will be small but relevant, in the range of -0.64 to 0.93 W/m^2 assuming 100% occurrence rate (with a single profile maximum of 4 W/m^2). Only aggregates for summer conditions have the potential for a net cooling effect. If a more realistic UTC coverage of 10 (20)% is assumed (Zou et al., 2020) the CRE is reduced to a still not irrelevant range of -0.06 (-0.12) to 0.09 (0.18) W/m^2.

The numbers of the radiative forcing caused by UTC calculated here can be put into perspective of the radiative forcing determined for CO_2 and other greenhouse gases. Myhre et al. (2009b) analysed in a similar designed study SW, LW, and net radiative effect of a stratospheric water vapour (SWV) enhancement as well as effects of contrail cirrus in a comparison of various radiative transport models. An overall global change of SWV from 3.0 to 3.7 ppmv has resulted in a net RF (LW+SW) of 0.22 to 0.49 W/m^2 depending on the specific model. This is of similar value and range as the mean 100% cloud cover-based - clearly an overestimate for the real atmosphere - CRE results for UTCs presented above. A typical contrail cirrus with optical depth of 0.3 and 100% coverage resulted in a CRE of -14 to -7 W/m^2 for high SZA (75°) and positive CRE of 12 - 23 W/m^2 for low SZA (30°). Similar to the UTCs focused on for this study, the CRE of optically thin contrails is very sensitive to the SZA, depending on the sunlight hours and the maximum SZA the overall CRE can change from negative to positive effects. Finally, Myhre et al. did a more realistic estimate of the global coverage of contrails and the resulting CRE. Four models deliver a rather good consistency in the range of 9.3 to 15 mW/m^2 (warming), which is significantly smaller than the estimates found above for 10 and 20% coverage of global UTCs. Only, if we further reduce the global coverage to 1% (to be consistent with the contrails coverage) the CRE of UTCs is in the range of -6 to $+9$ mW/m^2, where the warming of aggregates fits well with the contrails. However, these estimates indicate a significant larger CRE for UTCs than contrails.

Although the presented study specifies only first estimates for the CRE under various conditions, the results presented here show the priority to better constrain the amount (coverage) and vertical thickness of UTCs in the lower stratosphere and tropopause region. This would help to determine how important it is to consider UTCs in future climate model simulations. This

https://doi.org/10.5194/egusphere-2023-1234
Preprint. Discussion started: 19 June 2023
© Author(s) 2023. CC BY 4.0 License.

would also help to prove if UTCs are at least to some extent considered in the current very common cloud dataset composed from radar and lidar space measurements (e.g. Delanoë and Hogan, 2008; Deng et al., 2010).

5 Summary and Conclusions

The present study reports the radiative effect of optically ultra thin cirrus clouds. Our sensitivity simulations with different ice particle sizes and shapes for those clouds provide an uncertainty range for their RE during both summer and winter months. Cloud top height and ice water content are based on CRISTA-2 retrievals, while the cloud vertical thicknesses were assumed to be 0.5 or 2 km. Most of the model scenarios result in a positive cloud radiative effect (warming) in the mean range of -0.64 to 0.96 W/m^2 (Tab.1) for 100% cloud coverage. Only ice aggregates showed the ability to change the sign of CRE from warming to cooling. Summer conditions with extended sunlit hours are producing large cooling rates over the day so that the SW cooling effect is dominating the LW warming effect. Overall, the cooling and warming effects are nearly in balance for UTCs and the typical uncertainties of the various input parameters of the radiative transport calculation (e.g. particle type, effective radius or cloud layer thickness) makes it problematic to reliably quantify the net radiative effect.

So far UTCs are an unnoticed cirrus cloud type in many fields from cloud microphysical modelling to the parameterisation of the formation processes for various types in global models. Further investigations on the particle shape, effective radius, cloud coverage, and vertical thickness of UTCs are suggested here to minimize the uncertainties in the radiative transport calculations. Finally, such work should allow a more accurate quantification of the cooling or warming potential of UTCs which is so far not included in climate models.

Code and data availability. SOCRATES is a model hosted by the UK Meteorological Office and accessible after registration from https://code.metoffice.gov.uk/trac/socrates/wiki. Model input (CRISTA-2 and meteorological reanalysis data) and output data by SOCRATES used in this study are available on request from the first author. In addition, all program codes in IDL used for the data analysis are available from the first author.

Author contributions. All authors designed the study. RS analysed and prepared the CRISTA data for the model runs. AR performed the SOCRATES runs and prepared the output files for radiative effect calculations. RS together with AR analysed the model output. All authors contributed to data interpretation and writing of the paper.

Competing interests. At least one of the (co-)authors is a member of the editorial board of Atmospheric Chemistry and Physics.

https://doi.org/10.5194/egusphere-2023-1234
Preprint. Discussion started: 19 June 2023
© Author(s) 2023. CC BY 4.0 License.

Acknowledgements. The authors like to thank D. Offermann and the former CRISTA team at the University of Wuppertal, Germany, for the realization of two successful instrument missions and the subsequent data processing. Thanks to the UK Meteorological Office for providing and supporting the SOCRATES radiative transport model. The authors are grateful to the European Centre for Medium-Range Weather Forecasts (ECMWF) for providing reanalysis data.

https://doi.org/10.5194/egusphere-2023-1234
Preprint. Discussion started: 19 June 2023
© Author(s) 2023. CC BY 4.0 License.

References

Baran, A. J.: Simulation of infrared scattering from ice aggregates by use of a size-shape distribution of circular ice cylinders, Appl. Opt., 42, 2811–2818, https://doi.org/10.1364/AO.42.002811, 2003.

Baran, A. J. and Francis, P. N.: On the radiative properties of cirrus cloud at solar and thermal wavelengths: A test of model consistency using high-resolution airborne radiance measurements, Quarterly Journal of the Royal Meteorological Society, 130, 763–778, https://doi.org/https://doi.org/10.1256/qj.03.151, 2004.

Baran, A. J., Hill, P., Furtado, K., Field, P., and Manners, J.: A Coupled Cloud Physics–Radiation Parameterization of the Bulk Optical Properties of Cirrus and Its Impact on the Met Office Unified Model Global Atmosphere 5.0 Configuration, Journal of Climate, 27, 7725 – 7752, https://doi.org/10.1175/JCLI-D-13-00700.1, 2014.

Baran, A. J., Hill, P., Walters, D., Hardiman, S. C., Furtado, K., Field, P. R., and Manners, J.: The Impact of Two Coupled Cirrus Microphysics–Radiation Parameterizations on the Temperature and Specific Humidity Biases in the Tropical Tropopause Layer in a Climate Model, Journal of Climate, 29, 5299 – 5316, https://doi.org/10.1175/JCLI-D-15-0821.1, 2016.

Bartolome Garcia, I., Spang, R., Ungermann, J., Griessbach, S., Krämer, M., Höpfner, M., and Riese, M.: Observation of cirrus clouds with GLORIA during the WISE campaign: detection methods and cirrus characterization, Atmospheric Measurement Techniques, 14, 3153–3168, https://doi.org/10.5194/amt-14-3153-2021, 2021.

Davis, S., Hlavka, D., Jensen, E., Rosenlof, K., Yang, Q., Schmidt, S., Borrmann, S., Frey, W., Lawson, P., Voemel, H., and Bui, T. P.: In situ and lidar observations of tropopause subvisible cirrus clouds during TC4, Journal of Geophysical Research: Atmospheres, 115, https://doi.org/https://doi.org/10.1029/2009JD013093, 2010.

Delanoë, J. and Hogan, R. J.: A variational scheme for retrieving ice cloud properties from combined radar, lidar, and infrared radiometer, Journal of Geophysical Research: Atmospheres, 113, https://doi.org/https://doi.org/10.1029/2007JD009000, 2008.

Deng, M., Mace, G. G., Wang, Z., and Okamoto, H.: Tropical Composition, Cloud and Climate Coupling Experiment validation for cirrus cloud profiling retrieval using CloudSat radar and CALIPSO lidar, Journal of Geophysical Research: Atmospheres, 115, https://doi.org/https://doi.org/10.1029/2009JD013104, 2010.

Edwards, J. M. and Slingo, A.: Studies with a flexible new radiation code. I: Choosing a configuration for a large-scale model, Q. J. R. Meteorol. Soc., 122, 689–719, https://doi.org/10.1002/qj.49712253107, 1996.

Fischer, H., Birk, M., Blom, C., Carli, B., Carlotti, M., von Clarmann, T., Delbouille, L., Dudhia, A., Ehhalt, D., Endemann, M., Flaud, J. M., Gessner, R., Kleinert, A., Koopmann, R., Langen, J., López-Puertas, M., Mosner, P., Nett, H., Oelhaf, H., Perron, G., Remedios, J., Ridolfi, M., Stiller, G., and Zander, R.: MIPAS: An instrument for atmospheric and climate resaerch, Atmos. Chem. Phys., 8, https://doi.org/10.5194/acp-8-2151-2008, 2008.

Forster, P., Storelvmo, T., Armour, K., Collins, W., Dufresne, J.-L., Frame, D., Lunt, D., Mauritsen, T., Palmer, M., Watanabe, M., Wild, M., and Zhang, H.: The Earth's Energy Budget, Climate Feedbacks, and Climate Sensitivity, p. 923–1054, Cambridge University Press, Cambridge, United Kingdom and New York, NY, USA, https://doi.org/10.1017/9781009157896.009, 2021.

Grossmann, K. U., Offermann, D., Gusev, O., Oberheide, J., Riese, M., and Spang, R.: The CRISTA-2 Mission, J. Geophys. Res., 107, https://doi.org/10.1029/2001JD000667, 2002.

Hersbach, H., Bell, B., Berrisford, P., Hirahara, S., Horányi, A., Muñoz-Sabater, J., Nicolas, J., Peubey, C., Radu, R., Schepers, D., Simmons, A., Soci, C., Abdalla, S., Abellan, X., Balsamo, G., Bechtold, P., Biavati, G., Bidlot, J., Bonavita, M., De Chiara, G., Dahlgren, P., Dee, D., Diamantakis, M., Dragani, R., Flemming, J., Forbes, R., Fuentes, M., Geer, A., Haimberger, L., Healy, S., Hogan, R. J., Hólm, E.,

https://doi.org/10.5194/egusphere-2023-1234
Preprint. Discussion started: 19 June 2023
© Author(s) 2023. CC BY 4.0 License.

Janisková, M., Keeley, S., Laloyaux, P., Lopez, P., Lupu, C., Radnoti, G., de Rosnay, P., Rozum, I., Vamborg, F., Villaume, S., and Thépaut, J.-N.: The ERA5 global reanalysis, Q. J. R. Meteorol. Soc., 146, 1999–2049, https://doi.org/10.1002/qj.3803, 2020.

Heymsfield, A. J., Krämer, M., Luebke, A., Brown, P., Cziczo, D. J., Franklin, C., Lawson, P., Lohmann, U., McFarquhar, G., Ulanowski, Z., and Tricht, K. V.: Cirrus Clouds, Meteorological Monographs, 58, 2.1 – 2.26, https://doi.org/10.1175/AMSMONOGRAPHS-D-16-0010.1, 2017.

Hoffmann, L. and Spang, R.: An assessment of tropopause characteristics of the ERA5 and ERA-Interim meteorological reanalyses, Atmospheric Chemistry and Physics, 22, 4019–4046, https://doi.org/10.5194/acp-22-4019-2022, 2022.

Hong, Y. and Liu, G.: The Characteristics of Ice Cloud Properties Derived from CloudSat and CALIPSO Measurements, Journal of Climate, 28, 3880 – 3901, https://doi.org/10.1175/JCLI-D-14-00666.1, 2015.

Hong, Y., Liu, G., and Li, J.-L. F.: Assessing the Radiative Effects of Global Ice Clouds Based on CloudSat and CALIPSO Measurements, J. Climate, 29, 7651–7674, https://doi.org/10.1175/JCLI-D-15-0799.1, 2016.

Krämer, M., Rolf, C., Luebke, A., Afchine, A., Spelten, N., Costa, A., Meyer, J., Zöger, M., Smith, J., Herman, R. L., Buchholz, B., Ebert, V., Baumgardner, D., Borrmann, S., Klingebiel, M., and Avallone, L.: A microphysics guide to cirrus clouds – Part 1: Cirrus types, Atmos. Chem. Phys., 16, 3463–3483, https://doi.org/10.5194/acp-16-3463-2016, 2016.

Krämer, M., Rolf, C., Spelten, N., Afchine, A., Fahey, D., Jensen, E., Khaykin, S., Kuhn, T., Lawson, P., Lykov, A., Pan, L. L., Riese, M., Rollins, A., Stroh, F., Thornberry, T., Wolf, V., Woods, S., Spichtinger, P., Quaas, J., and Sourdeval, O.: A microphysics guide to cirrus – Part 2: Climatologies of clouds and humidity from observations, Atmospheric Chemistry and Physics, 20, 12 569–12 608, https://doi.org/10.5194/acp-20-12569-2020, 2020.

Kunz, A., Müller, R., Homonnai, V., Jánosi, I., Hurst, D., Rap, A., Forster, P., Rohrer, F., Spelten, N., and Riese, M.: Extending water vapor trend observations over Boulder into the tropopause region: trend uncertainties and resulting radiative forcing, J. Geophys. Res., 118, 11 269–11 284, https://doi.org/10.1002/jgrd.50831, 2013.

Lawson, R. P., Woods, S., Jensen, E., Erfani, E., Gurganus, C., Gallagher, M., Connolly, P., Whiteway, J., Baran, A. J., May, P., Heymsfield, A., Schmitt, C. G., McFarquhar, G., Um, J., Protat, A., Bailey, M., Lance, S., Muehlbauer, A., Stith, J., Korolev, A., Toon, O. B., and Krämer, M.: A Review of Ice Particle Shapes in Cirrus formed In Situ and in Anvils, Journal of Geophysical Research: Atmospheres, 124, 10 049–10 090, https://doi.org/https://doi.org/10.1029/2018JD030122, 2019.

Liou, K.-N.: Influence of Cirrus Clouds on Weather and Climate Processes: A Global Perspective, Monthly Weather Review, 114, 1167 – 1199, https://doi.org/10.1175/1520-0493(1986)114<1167:IOCCOW>2.0.CO;2, 1986.

Massie, S. T., Gille, J., Craig, C., Khosravi, R., Barnett, J., Read, W., and Winker, D.: HIRDLS and CALIPSO observations of tropical cirrus, Journal of Geophysical Research: Atmospheres, 115, https://doi.org/https://doi.org/10.1029/2009JD012100, 2010.

McFarquhar, G. M., Yang, P., Macke, A., and Baran, A. J.: A New Parameterization of Single Scattering Solar Radiative Properties for Tropical Anvils Using Observed Ice Crystal Size and Shape Distributions, Journal of the Atmospheric Sciences, 59, 2458 – 2478, https://doi.org/10.1175/1520-0469(2002)059<2458:ANPOSS>2.0.CO;2, 2002.

Myhre, G., Berglen, T. F., Johnsrud, M., Hoyle, C. R., Berntsen, T. K., Christopher, S. A., Fahey, D. W., Isaksen, I. S. A., Jones, T. A., Kahn, R. A., Loeb, N., Quinn, P., Remer, L., Schwarz, J. P., and Yttri, K. E.: Modelled radiative forcing of the direct aerosol effect with multi-observation evaluation, Atmospheric Chemistry and Physics, 9, 1365–1392, https://doi.org/10.5194/acp-9-1365-2009, 2009a.

https://doi.org/10.5194/egusphere-2023-1234
Preprint. Discussion started: 19 June 2023
© Author(s) 2023. CC BY 4.0 License.

Myhre, G., Kvalevg, M., Rädel, G., Cook, J., Shine, K. P., Clark, H., Karcher, F., Markowicz, K., Kardas, A., Wolkenberg, P., Balkanski, Y., Ponater, M., Forster, P., Rap, A., and Leon, R. R.: Intercomparison of radiative forcing calculations of stratospheric water vapour and contrails, Meteorologische Zeitschrift, 18, 585–596, https://doi.org/10.1127/0941-2948/2009/0411, 2009b.

Offermann, D., Grossmann, K.-U., Barthol, P., Knieling, P., Riese, M., and Trant, R.: Cryogenic Infrared Spectrometers and Telescopes for the Atmosphere (CRISTA) experiment and middle atmosphere variability, J. Geophys. Res., 104, 16,311–16,325, 1999.

Peter, T., Luo, B. P., Wirth, M., Kiemle, C., Flentje, H., Yushkov, V. A., Khattatov, V., Rudakov, V., Thomas, A., Borrmann, S., Toci, G., Mazzinghi, P., Beuermann, J., Schiller, C., Cairo, F., Di Donfrancesco, G., Adriani, A., Volk, C. M., Strom, J., Noone, K., Mitev, V., MacKenzie, R. A., Carslaw, K. S., Trautmann, T., Santacesaria, V., and Stefanutti, L.: Ultrathin Tropical Tropopause Clouds (UTTCs): I. Cloud morphology and occurrence, Atmospheric Chemistry and Physics, 3, 1083–1091, https://doi.org/10.5194/acp-3-1083-2003, 2003.

Rap, A., Forster, P. M., Jones, A., Boucher, O., Haywood, J. M., Bellouin, N., and De Leon, R. R.: Parameterization of contrails in the UK Met Office Climate Model, Journal of Geophysical Research: Atmospheres, 115, https://doi.org/https://doi.org/10.1029/2009JD012443, 2010.

Rap, A., Scott, C. E., Spracklen, D. V., Bellouin, N., Forster, P. M., Carslaw, K. S., Schmidt, A., and Mann, G.: Natural aerosol direct and indirect radiative effects, Geophysical Research Letters, 40, 3297–3301, https://doi.org/https://doi.org/10.1002/grl.50441, 2013.

Rap, A., Richards, N. A. D., Forster, P. M., Monks, S. A., Arnold, S. R., and Chipperfield, M. P.: Satellite constraint on the tropospheric ozone radiative effect, Geophysical Research Letters, 42, 5074–5081, https://doi.org/https://doi.org/10.1002/2015GL064037, 2015a.

Rap, A., Spracklen, D. V., Mercado, L., Reddington, C. L., Haywood, J. M., Ellis, R. J., Phillips, O. L., Artaxo, P., Bonal, D., Restrepo Coupe, N., and Butt, N.: Fires increase Amazon forest productivity through increases in diffuse radiation, Geophysical Research Letters, 42, 4654–4662, https://doi.org/https://doi.org/10.1002/2015GL063719, 2015b.

Rap, A., Scott, C., Reddington, C., Mercado, L., Ellis, R., Garraway, S., Evans, M., Beerling, D., MacKenzie, A., Hewitt, C., and Spracklen, D.: Enhanced global primary production by biogenic aerosol via diffuse radiation fertilization, Nature Geosci., 11, 640—-644, https://doi.org/https://doi.org/10.1038/s41561-018-0208-3, 2018.

Riese, M., Ploeger, F., Rap, A., Vogel, B., Konopka, P., Dameris, M., and Forster, P.: Impact of uncertainties in atmospheric mixing on simulated UTLS composition and related radiative effects, J. Geophys. Res., 117, D16305, https://doi.org/10.1029/2012JD017751, 2012.

Riese, M., Oelhaf, H., Preusse, P., Blank, J., Ern, M., Friedl-Vallon, F., Fischer, H., Guggenmoser, T., Höpfner, M., Hoor, P., Kaufmann, M., Orphal, J., Plöger, F., Spang, R., Sumińska-Ebersoldt, O., Ungermann, J., Vogel, B., and Woiwode, W.: Gimballed Limb Observer for Radiance Imaging of the Atmosphere (GLORIA) scientific objectives, Atmos. Meas. Tech., 7, 1915–1928, https://doi.org/10.5194/amt-7-1915-2014, 2014.

Rother, T., Schmidt, K., Wauer, J., Shcherbakov, V., and Gayet, J.-F.: Light scattering on Chebyshev particles of higher order, Appl. Opt., 45, 6030–6037, https://doi.org/10.1364/AO.45.006030, 2006.

Sassen, K. and Cho, B. S.: Subvisual-thin cirrus lidar data set for satellite verification and climatological research, J. Appl. Meteorol., 31, 1275–1285, https://doi.org/https://doi.org/10.1175/1520-0450(1992)031<1275:STCLDF>2.0.CO;2, 1992.

Spang, R., Eidmann, G., Riese, M., Offermann, D., Preusse, P., Pfister, L., and Wang, P.-H.: CRISTA observations of cirrus clouds around the tropopause, Journal of Geophysical Research: Atmospheres, 107, CRI 2–1–CRI 2–18, https://doi.org/https://doi.org/10.1029/2001JD000698, 2002.

Spang, R., Remedios, J., and Barkley, M.: Colour indices for the detection and differentiation of cloud types in infra-red limb emission spectra, Advances in Space Research, 33, 1041–1047, https://doi.org/https://doi.org/10.1016/S0273-1177(03)00585-4, climate Change Processes in the Stratosphere, Earth-Atmosphere-Ocean Systems, and Oceanographic Processes from Satellite Data, 2004.

https://doi.org/10.5194/egusphere-2023-1234
Preprint. Discussion started: 19 June 2023
© Author(s) 2023. CC BY 4.0 License.

Spang, R., Hoffmann, L., Kullmann, A., Olschewski, F., Preusse, P., Knieling, P., Schroeder, S., Stroh, F., Weigel, K., and Riese, M.: High resolution limb observations of clouds by the CRISTA-NF experiment during the SCOUT-O3 tropical aircraft campaign, Advances in Space Research, 42, 1765–1775, https://doi.org/https://doi.org/10.1016/j.asr.2007.09.036, 2008.

Spang, R., Arndt, K., Dudhia, A., Höpfner, M., Hoffmann, L., Hurley, J., Grainger, R. G., Griessbach, S., Poulsen, C., Remedios, J. J., Riese, M., Sembhi, H., Siddans, R., Waterfall, A., and Zehner, C.: Fast cloud parameter retrievals of MIPAS/Envisat, Atmos. Chem. Phys., 12, 7135–7164, https://doi.org/10.5194/acp-12-7135-2012, 2012.

Spang, R., Günther, G., Riese, M., Hoffmann, L., Müller, R., and Griessbach, S.: Satellite observations of cirrus clouds in the Northern Hemisphere lowermost stratosphere, Atmospheric Chemistry and Physics, 15, 927–950, https://doi.org/10.5194/acp-15-927-2015, 2015.

Ungermann, J., Bartolome, I., Griessbach, S., Spang, R., Rolf, C., Krämer, M., Höpfner, M., and Riese, M.: Cirrus cloud shape detection by tomographic extinction retrievals from infrared limb emission sounder measurements, Atmospheric Measurement Techniques, 13, 7025–7045, https://doi.org/10.5194/amt-13-7025-2020, 2020.

Woods, S., Lawson, R. P., Jensen, E., Bui, T. P., Thornberry, T., Rollins, A., Pfister, L., and Avery, M.: Microphysical Properties of Tropical Tropopause Layer Cirrus, Journal of Geophysical Research: Atmospheres, 123, 6053–6069, https://doi.org/https://doi.org/10.1029/2017JD028068, 2018.

Yang, E.-S., Cunnold, D. M., Newchurch, M. J., and Salawitch, R. J.: Change in ozone trends at southern high latitudes, Geophys. Res. Lett., 32, L12812, https://doi.org/doi:10.1029/2004GL022296, 2005.

Yang, P., Baum, B. A., Heymsfield, A. J., Hu, Y. X., Huang, H.-L., Tsay, S.-C., and Ackerman, S.: Single-scattering properties of droxtals, Journal of Quantitative Spectroscopy and Radiative Transfer, 79-80, 1159–1169, https://doi.org/https://doi.org/10.1016/S0022-4073(02)00347-3, electromagnetic and Light Scattering by Non-Spherical Particles, 2003.

Yi, B., Yang, P., Baum, B. A., L'Ecuyer, T., Oreopoulos, L., Mlawer, E. J., Heymsfield, A. J., and Liou, K.-N.: Influence of Ice Particle Surface Roughening on the Global Cloud Radiative Effect, Journal of the Atmospheric Sciences, 70, 2794 – 2807, https://doi.org/10.1175/JAS-D-13-020.1, 2013.

Zhang, Z., Yang, P., Kattawar, G. W., Tsay, S.-C., Baum, B. A., Hu, Y., Heymsfield, A. J., and Reichardt, J.: Geometrical-optics solution to light scattering by droxtal ice crystals, Appl. Opt., 43, 2490–2499, https://doi.org/10.1364/AO.43.002490, 2004.

Zou, L., Griessbach, S., Hoffmann, L., Gong, B., and Wang, L.: Revisiting global satellite observations of stratospheric cirrus clouds, Atmos. Chem. Phys., 20, 9939–9959, https://doi.org/10.5194/acp-20-9939-2020, 2020.

Zou, L., Hoffmann, L., Griessbach, S., Spang, R., and Wang, L.: Empirical evidence for deep convection being a major source of stratospheric ice clouds over North America, Atmos. Chem. Phys., 21, 10 457–10 475, https://doi.org/10.5194/acp-21-10457-2021, 2021.

Zou, L., Griessbach, S., Hoffmann, L., and Spang, R.: A global view on stratospheric ice clouds: assessment of processes related to their occurrence based on satellite observations, Atmospheric Chemistry and Physics, 22, 6677–6702, https://doi.org/10.5194/acp-22-6677-2022, 2022.